CHEMISTRY
A EUROPEAN JOURNAL

DOI: 10.1002/chem.201100493

Intermolecular and Intracomplex Photoinduced Electron Transfer from Planar and Nonplanar Metalloporphyrins to *p*-Quinones

Masanori Kanematsu,[a] Panče Naumov,[a, b] Takahiko Kojima,*[c] and Shunichi Fukuzumi*[a, d]

Abstract: The rate constants of intermolecular photoinduced electron transfer from triplet excited states of metalloporphyrins to a series of *p*-benzoquinone derivatives in benzonitrile were determined to examine the effects of the driving force, the metal, and the conformational distortion of the porphyrin ring on the reorganization energies (λ) of electron transfer by laser flash photolysis. The λ values were evaluated from the determined rate constants on the basis of the Marcus theory of electron transfer. The λ values of planar metalloporphyrins, [Al(TPP)(PhCO*O*)] and [Zn(TPP)] (TPP^{2-} = tetraphenylporphyrin dianion), are approximately the same, but they are 0.27 eV smaller than those of the corresponding nonplanar (saddle-distorted) metalloporphyrins [Al(DPP)(PhCO*O*)] and [Zn(DPP)] (DPP^{2-} = dodecaphenylporphyrin dianion) when they are compared for the same driving force of photoinduced electron transfer. The axial ligand $PhCOO^-$ of $[Al(TPP)]^+$ and $[Al(DPP)]^+$ was replaced by anthraquinone-2-carboxylate ($AqCOO^-$) to afford the electron donor–acceptor complexes [Al(TPP)(AqCO*O*)] and [Al(DPP)(AqCO*O*)], respectively. The X-ray crystal structure of [Al(TPP)(AqCO*O*)] revealed strong coordination of $AqCOO^-$ to the Al^{3+} ion of $[Al(TPP)]^+$ and the existence of π–π interactions between $AqCOO^-$ and the porphyrin ring. In the case of the saddle-distorted [Al(DPP)(AqCO*O*)], however, the $AqCOO^-$ moiety is nearly perpendicular to the porphyrin ring. The photodynamics of intracomplex photoinduced electron transfer from the singlet excited state of $[Al(TPP)]^+$ and $[Al(DPP)]^+$ to the $AqCOO^-$ moiety were also examined in comparison with the intermolecular photoinduced electron-transfer reactions, and the determined rate constants were evaluated in light of the Marcus theory of electron transfer to reveal that the electron transfer is adiabatic in each case.

Keywords: electron transfer · photochemistry · photosynthesis · pi interactions · redox chemistry

Introduction

Electron transfer is the most fundamental chemical process in which an electron moves from one molecule to another, playing an important role not only in chemistry, but also in biological processes such as photosynthesis and respiration.[1,2] Electron-transfer reactions commonly involve transition metal complexes, but there are now many examples of electron-transfer reactions in organic chemistry.[3–9] Intermolecular rate constants (k_{et}) of outer-sphere electron-transfer reactions have been well predicted by the Marcus theory of electron transfer using Equation (1),[10] in which k_{diff} is the diffusion rate constant, Z is the collision frequency (normally taken as $1\times10^{11}\,M^{-1}s^{-1}$), ΔG_{et} is the free-energy change of electron transfer, and λ is the reorganization energy of electron transfer (the energy required to structurally reorganize the donor, acceptor, and their solvation spheres upon electron transfer).

$$k_{et} = [k_{diff}^{-1} + Z^{-1}\exp\{(\frac{\lambda}{4})\frac{(1+\Delta G_{et}/\lambda)^2}{k_B T}\}]^{-1} \quad (1)$$

The driving force of electron transfer is given as the difference between the one-electron reduction potential (E_{red}) of an electron acceptor and the one-electron oxidation potential (E_{ox}) of an electron donor, as shown in Equation (2).[3–9]

[a] M. Kanematsu, Dr. P. Naumov, Prof. Dr. S. Fukuzumi
Department of Material and Life Science
Graduate School of Engineering, Osaka University
ALCA (Japan) Science and Technology Agency (JST)
2–1 Yamada-oka, Suita, Osaka 565-0871 (Japan)
Fax: (+81) 6-6879-7370
E-mail: fukuzumi@chem.eng.osaka-u.ac.jp

[b] Dr. P. Naumov
Frontier Research Base for Global Young Researchers
Graduate School of Engineering, Osaka University
2–1 Yamada-oka, Suita, Osaka 565-0871 (Japan)

[c] Prof. Dr. T. Kojima
Department of Chemistry
Graduate School of Pure and Applied Sciences
University of Tsukuba
1-1-1 Tennoudai, Tsukuba, Ibaraki 305-8571 (Japan)
E-mail: kojima@chem.tsukuba.ac.jp

[d] Prof. Dr. S. Fukuzumi
Department of Bioinspired Science
Ewha Womans University
Seoul 120-750 (Korea)

Supporting information for this article is available on the WWW under http://dx.doi.org/10.1002/chem.201001008.

$$\Delta G_{et} = e(E_{red} - E_{ox}) \quad (2)$$

Quantitative analyses of intermolecular electron-transfer reactions have mostly focused on outer-sphere electron-transfer processes,[11,12] in which the electronic coupling or binding energy within the elusive precursor complex is sufficiently weak to be neglected, but still strong enough to make the electron transfer in the precursor complex adiabatic so that the electron-transfer rate constant is determined solely by the driving force of the electron transfer ($-\Delta G_{et}$) and the reorganization energy (λ) in Equation (1). Thus, the observed electron-transfer rate is intrinsically insensitive to the interaction and geometry between an electron donor and acceptor pair in the precursor complex. In such a case, the λ value is the most important factor in determining the electron-transfer reactivity of electron donor and acceptor molecules besides the one-electron redox potentials.[1–12] There have so far been extensive studies on the λ values of a number of electron-transfer reactions of electron donor and acceptor molecules.[3,13,14]

Among numerous electron donor and acceptor molecules, porphyrins have merited special attention in relation to their important roles in biological electron-transfer systems such as photosynthesis and respiration.[1,2,15–17] Artificial photosynthetic systems composed of porphyrins linked with electron acceptors by covalent or noncovalent bonds have been studied extensively and applied to a variety of photofunctional materials, because of the efficient photoinduced electron transfer in porphyrin-based compounds.[18–25] In such porphyrin-based donor–acceptor linked systems, the electronic coupling between the donor and acceptor molecule is normally insufficient to make the electron transfer in the precursor complex adiabatic, and the rate constant is highly dependent on the geometry and the distance between the donor and acceptor molecules.[18–25] The electronic coupling generally becomes weaker in donor–acceptor coordination complexes linked by noncovalent bonding as compared with those linked by covalent bonding.[21–25] Thus, there has been no report on adiabatic photoinduced electron transfer in donor–acceptor coordination complexes with X-ray crystal structures.

The electron-transfer reactivity of porphyrins can be finely tuned by conformational distortion of the porphyrin ligand, the central metal, and the axial coordination.[26,27] For example, the rates of photoinduced electron-transfer reactions of diprotonated porphyrins that act as electron acceptors are significantly slowed down by conformational distortion of the porphyrin ring, which results in a large increase in the reorganization energy of electron transfer.[27] Such nonplanar conformations of porphyrins are known to influence not only the photophysical and redox properties of synthetic porphyrins, but also the biological functions of various porphyrinoids in metalloproteins.[28,29] However, the effects of conformational distortion of the porphyrin ligand on intermolecular or intramolecular electron-transfer reactions of metalloporphyrins that act as electron donors have yet to be reported. There has been no systematic study on the effects of the driving force, the central metal, the axial ligand, and the conformational distortion of the porphyrin ring on the reorganization energies of the intermolecular or intramolecular electron transfer of metalloporphyrins.

Herein, we report the first systematic study on the dynamics of intermolecular electron-transfer reactions of planar and nonplanar metalloporphyrins using a series of *p*-benzoquinone derivatives as electron acceptors (Scheme 1) to examine the effects of the driving force, the central metal, the axial ligand, and the conformational distortion of the porphyrin ring on the reorganization energies of electron transfer. Planar and nonplanar Al^{III} porphyrins with an axial ligand ($PhCOO^-$), [Al(TPP)(PhCO*O*)] (TPP^{2-} = tetraphenylporphyrin dianion) and [Al(DPP)(PhCO*O*)] (DPP^{2-} = dodecaphenylporphyrin dianion), were employed to examine the effects of conformational distortion of the porphyrin ligand and the axial ligand in comparison with the corresponding Zn^{II} porphyrins, [Zn(TPP)] and [Zn(DPP)], respectively. It should be noted that there have been only a few reports on the photoinduced electron-transfer reactions of Al^{III} porphyrins.[30,31]

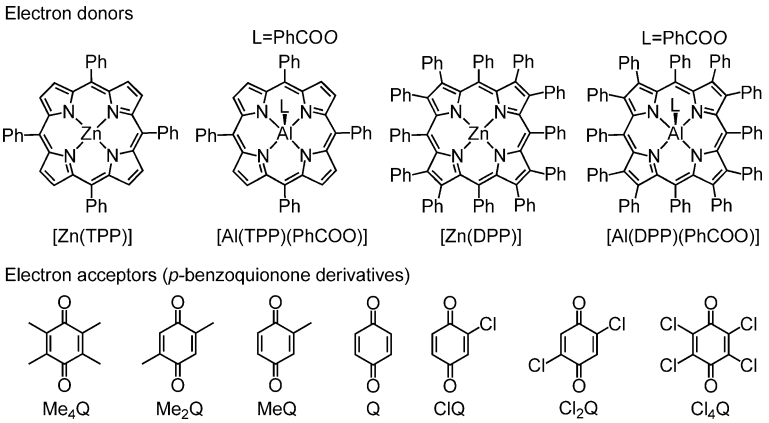

Scheme 1. Structures of metalloporphyrins and *p*-benzoquinone derivatives.

The intracomplex photoinduced electron-transfer reactions of $[Al(TPP)]^+$ and $[Al(DPP)]^+$ were also examined by replacing the $PhCOO^-$ axial ligand with anthraquinone-2-carboxylate ($AqCOO^-$), which can act as an electron acceptor (Scheme 2). The strong Lewis acidity of the Al^{3+} ion enables the formation of strong axial ligand binding of $AqCOO^-$. The difference in the binding geometries between [Al(TPP)(AqCO*O*)] and [Al(DPP)(AqCO*O*)] in Scheme 2

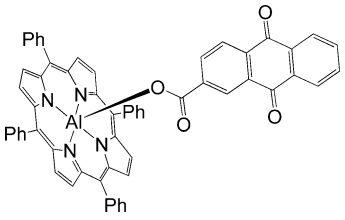

[Al(TPP)(AqCO*O*)]

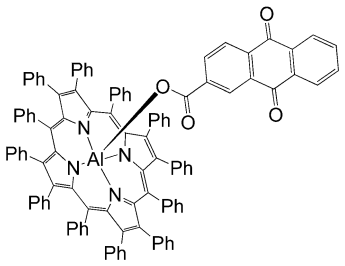

[Al(DPP)(AqCO*O*)]

Scheme 2. Structures of [Al(TPP)(AqCO*O*)] and [Al(DPP)(AqCO*O*)].

is revealed by the X-ray crystal structures, which have been successfully determined in this study.

The dynamics of both intermolecular and intracomplex photoinduced electron-transfer reactions of metalloporphyrins with *p*-benzoquinone derivatives (Schemes 1 and 2) were investigated by laser flash photolysis measurements. The resulting rate constants of photoinduced electron transfer were evaluated in light of the Marcus theory of electron transfer to reveal that this is the first example of adiabatic photoinduced electron transfer in electron donor–acceptor coordination complexes ([Al(TPP)(AqCO*O*)] and [Al(DPP)(AqCO*O*)]) with X-ray crystal structures. The λ values, which were determined in the present study, are found to depend on the driving force, central metal, axial ligand, and conformational distortion of the porphyrin ring, providing valuable insights for the rational design of electron-transfer systems of metalloporphyrins.

Results and Discussion

Photoinduced electron-transfer dynamics: Time-resolved nanosecond transient absorption spectra of metalloporphyrins were measured in the presence of *p*-benzoquinone derivatives to examine the dynamics of intermolecular photoinduced electron transfer from the triplet excited state of metalloporphyrins to *p*-benzoquinone derivatives in deaerated PhCN at 298 K. Figure 1 a shows the transient absorption spectral change of [Al(TPP)(PhCO*O*)] with *p*-chloranil (Cl_4Q) as a typical electron acceptor. The T–T absorption band at 490 nm due to ^{3}[Al(TPP)(PhCO*O*)]* decays, accompanied by the rise of an absorption band at 410 nm due to $Cl_4Q^{\bullet-}$,[32] together with a broad absorption band in the region of 600–800 nm due to [Al(TPP$^{\bullet+}$)(PhCO*O*)] (Figures 1 a–c). The assignment of the broad absorption band in the region of 600–800 nm was made through comparison with the differential absorption spectrum obtained by the one-electron oxidation of [Al(TPP)(PhCO*O*)] with a strong one-electron oxidant $[Ru(bpy)_3]^{3+}$ (Figure 1 d). Thus, electron transfer from ^{3}[Al(TPP)(PhCO*O*)]* to Cl_4Q to produce

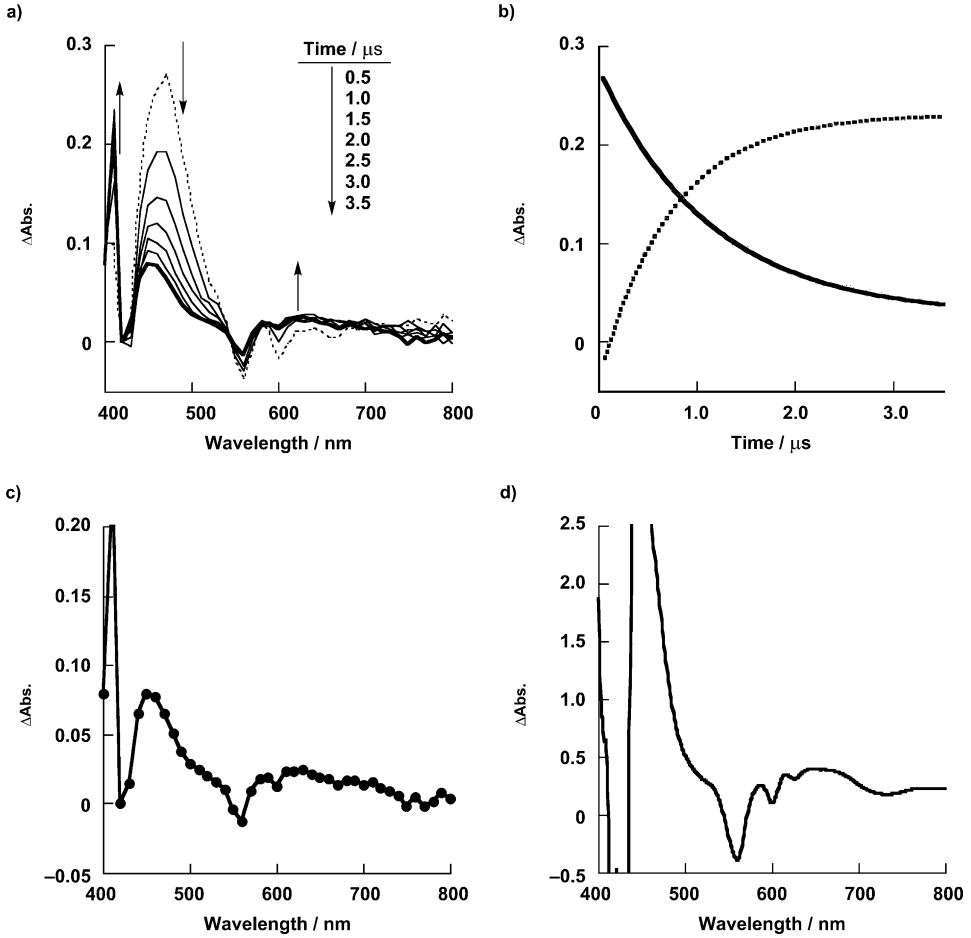

Figure 1. a) Transient absorption spectra of [Al(TPP)(PhCO*O*)] (3.0×10^{-5} M) in the presence of Cl_4Q (1.6×10^{-4} M) in deaerated PhCN at 298 K after nanosecond laser excitation at 559 nm. b) Time profile at 410 nm (dotted line) and 490 nm (black line). c) Transient absorption spectrum of [Al(TPP)(PhCO*O*)] (3.0×10^{-5} M) in the presence of Cl_4Q (1.6×10^{-4} M) in deaerated PhCN at 298 K observed 3.5 μs after nanosecond laser excitation at 559 nm. d) Difference absorption spectrum of [Al(TPP$^{\bullet+}$)(PhCO*O*)] generated by the electron-transfer oxidation of [Al(TPP)(PhCO*O*)] (3.0×10^{-5} M) with $[Ru(bpy)_3]^{3+}$ (3.0×10^{-5} M) in deaerated PhCN at 298 K.

[Al(TPP$^{\bullet+}$)(PhCO*O*)] and $Cl_4Q^{\bullet-}$ was confirmed. The time profile indicates that the electron transfer proceeded simultaneously with the decay of the triplet excited state of [Al(TPP)(PhCO*O*)] (Figure 1b).

The occurrence of electron transfer from ^{3}[Al(DPP)(PhCO*O*)]* to Cl_4Q was also confirmed by the transient absorption spectrum of [Al(DPP)(PhCO*O*)] (3.0×10^{-5} M) in the presence of Cl_4Q (9.9×10^{-4} M) in deaerated PhCN at 298 K (Figure 2c) in comparison with the differential spectrum obtained by the one-electron oxidation of [Al(DPP)(PhCO*O*)] with a strong one-electron oxidant $[Ru(bpy)_3]^{3+}$ (Figure 2d). The transient absorption spectra of [Zn(TPP)] and [Zn(DPP)] as well as [Al(TPP)(PhCO*O*)] and [Al(DPP)(PhCO*O*)] in the presence of *p*-benzoquinone derivatives were also measured to confirm the occurrence of electron transfer from the triplet excited states to the *p*-benzoquinone derivatives (Figures S1 and S2 in the Supporting Information).

The rates of electron transfer from the triplet excited states of metalloporphyrins to the *p*-benzoquinone derivatives obeyed pseudo-first-order kinetics. A typical example is shown in Figure 3. The pseudo-first-order rate constant increased linearly with increasing concentration of methyl-*p*-benzoquinone (MeQ), as shown in Figure 3b. From the slope of the linear plot depicted in Figure 3b, the second-order rate constant (k_{et}) of intermolecular electron transfer from ^{3}[Al(TPP)(PhCO*O*)]* to MeQ was determined to be 1.2×10^9 M^{-1}s^{-1}. Even though the driving force is small or slightly negative, the photoinduced electron-transfer reaction is irreversible because back electron transfer to the ground state is faster than electron transfer from the excited state.[4,33] Similarly, the k_{et} values of electron transfer from the triplet excited state of other metalloporphyrins to *p*-benzoquinone derivatives were determined as listed in Table 1 (Figure S3 in the Supporting Information).

The driving forces ($-\Delta G^*_{et}$) of the photoinduced electron transfer from the triplet excited state of metalloporphyrins to the *p*-benzoquinone derivatives were determined from the one-electron oxidation potentials of the metalloporphyrins (E_{ox}), the one-electron reduction potentials of the *p*-benzoquinone derivatives (E_{red}), and the triplet energies ($E(T_1)$) using Equation (3), in which *e* is the elemental charge.

$$-\Delta G^*_{et} = e(E_{red} - E_{ox}) + E(T_1) \quad (3)$$

The $E(T_1)$ values were determined from the phosphorescence spectra of the metalloporphyrins as listed in Table 2 (Figures S4–S6 in the Supporting Information), where the E_{ox} values are also given, together with the one-electron reduction potentials of the *p*-benzoquinone derivatives. The electrostatic stabilization term is neglected in a highly polar solvent such as PhCN in Equation (3).[3,4]

Plots of $\log k_{et}$ of photoinduced electron transfer from ^{3}[Zn(TPP)]*, ^{3}[Zn(DPP)]*, ^{3}[Al(TPP)(PhCO*O*)]*, and ^{3}[Al(DPP)(PhCO*O*)]* to a series of *p*-benzoquinone derivatives are shown in Figures 4a and 4b, respectively. Each plot cannot be fitted with the same λ value using Equation (1), and the λ value increases with the increasing driving force of the photoinduced electron transfer. Such an increase in the λ value suggests that the mean distance between the porphyrin (donor) and acceptor molecules increases with increasing driving force

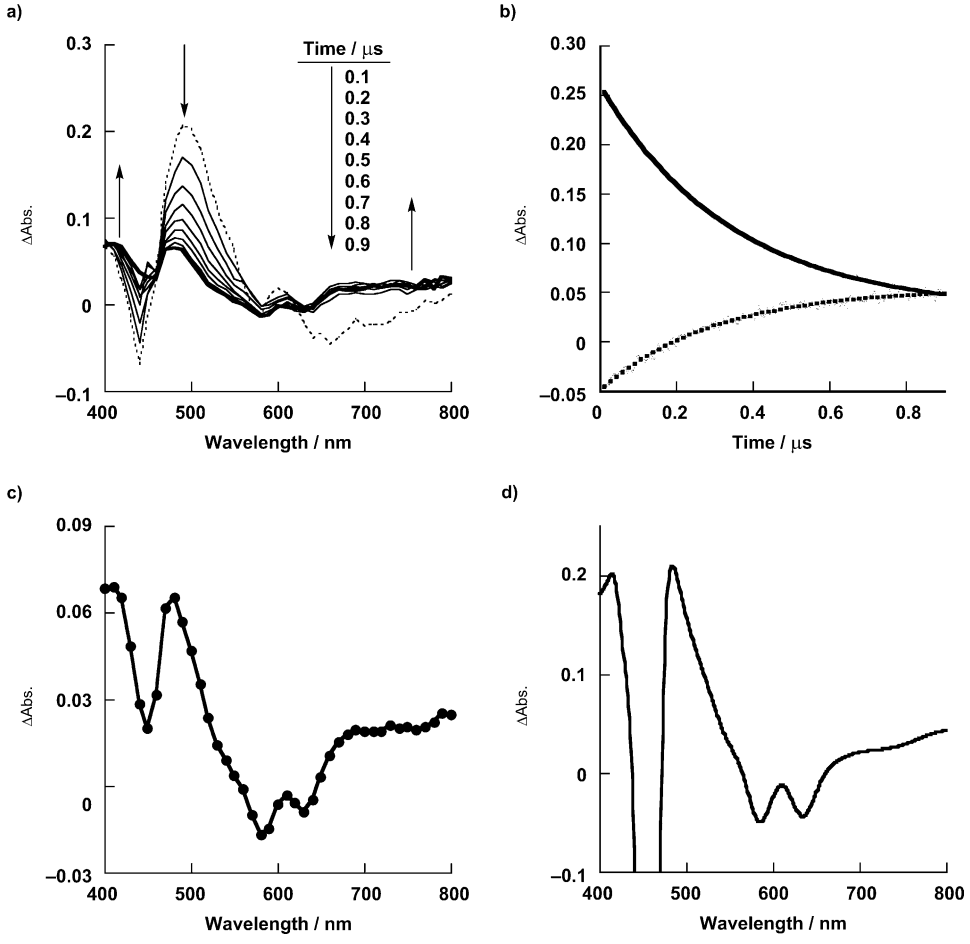

Figure 2. a) Transient absorption spectra of [Al(DPP)(PhCO*O*)] (3.0×10^{-5} M) in the presence of Cl_4Q (9.9×10^{-4} M) in deaerated PhCN at 298 K after nanosecond laser excitation at 585 nm. b) Time profile at 430 nm (dotted line) and 500 nm (black line). c) Transient absorption spectrum of [Al(DPP)(PhCO*O*)] (3.0×10^{-5} M) in the presence of Cl_4Q (9.9×10^{-4} M) in deaerated PhCN at 298 K observed 1.6 μs after nanosecond laser excitation at 585 nm. d) Difference absorption spectrum of [Al(DPP$^{\bullet+}$)(PhCO*O*)] generated by the electron-transfer oxidation of [Al(DPP)(PhCO*O*)] (4×10^{-6} M) with $[Ru(bpy)_3]^{3+}$ (4×10^{-6} M) in deaerated PhCN at 298 K.

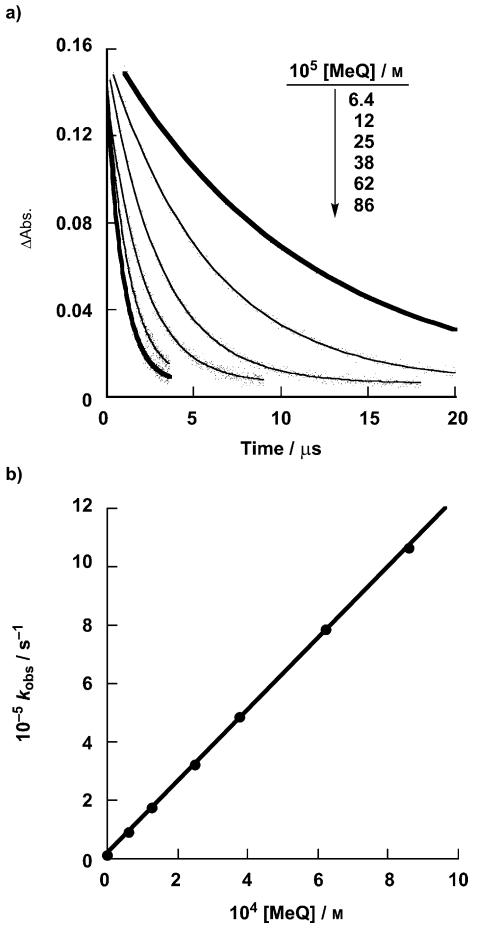

Figure 3. a) Decay time profiles at 500 nm of [Al(TPP)(PhCO*O*)] (3.0×10^{-5} M) in the presence of MeQ in deaerated PhCN at 298 K. b) Plot of the pseudo-first-order rate constant (k_{obs}) versus MeQ concentration.

Table 1. One-electron reduction potentials (E_{red}) of electron acceptors and rate constants (k_{et}) for electron transfer from ^{3}[Zn(TPP)]*, ^{3}[Al(TPP)(PhCO*O*)]*, ^{3}[Zn(DPP)]*, and ^{3}[Al(DPP)(PhCO*O*)]* to *p*-benzoquinone derivatives (electron acceptors) in PhCN at 298 K.

Electron acceptor	E_{red}[a] [V vs. SCE]	k_{et} [$M^{-1}s^{-1}$] [Zn(TPP)]	[Al(TPP)-(PhCO*O*)]	[Zn(DPP)]	[Al(TPP)-(PhCO*O*)]
Me_4Q	−0.96	3.2×10^8	–[b]	–[c]	–[c]
Me_2Q	−0.79	1.4×10^9	6.8×10^8	–[c]	–[c]
MeQ	−0.68	2.3×10^9	1.2×10^9	–[c]	–[c]
Q	−0.61	3.3×10^9	1.7×10^9	7.9×10^8	1.4×10^8
ClQ	−0.50	5.0×10^9	3.7×10^9	1.1×10^9	2.3×10^8
Cl_2Q	−0.29	5.0×10^9	3.9×10^9	1.7×10^9	4.5×10^8
Cl_4Q	−0.09	6.2×10^9	5.6×10^9	3.2×10^9	1.8×10^9

[a] Determined from cyclic voltammetry in PhCN containing 0.1 M $TBAPF_6$ at 298 K. [b] Not measured because of the excessively negative $-\Delta G_{et}$ value. [c] k_{et} values not determined because of the too poor acceleration of the decay of the triplet excited states.

Table 2. One-electron oxidation potentials (E_{ox}), and energies of singlet excited states ($E(S_1)$) and triplet excited states ($E(T_1)$) of metalloporphyrins.

Metalloporphyrin	E_{ox} [V vs. SCE][a]	$E(S_1)$ [eV][b]	$E(T_1)$ [eV]
[Zn(TPP)]	0.66	1.97	1.58[c]
[Al(TPP)(PhCO*O*)]	0.76	1.96	1.50[c]
[Zn(DPP)]	0.35	1.75	1.39[c]
[Al(DPP)(PhCO*O*)]	0.60	1.87	1.25[c]

[a] Determined from cyclic voltammetry in PhCN containing 0.1 M $TBAPF_6$ at 298 K (Figures S7–S10 in the Supporting Information). [b] Determined from the absorption and fluorescence spectra in PhCN at 298 K (Figures S11 and S12 in the Supporting Information). [c] Determined from the phosphorescence spectra in frozen 2-methyltetrahydrofuran at 77 K.[34]

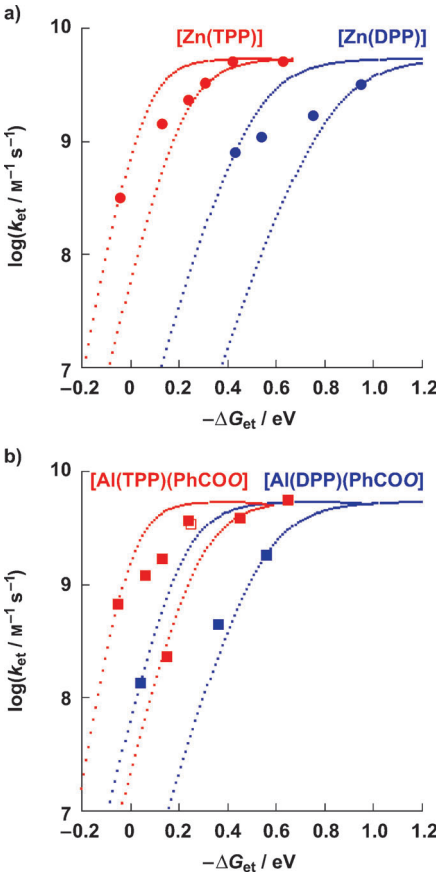

Figure 4. Dependence of $\log k_{et}$ on $-\Delta G_{et}$ for electron transfer from a) [Zn(TPP)] (●), [Zn(DPP)] (●), b) [Al(TPP)(PhCO*O*)] (■) and [Al(DPP)(PhCO*O*)] (■) to various electron acceptors in PhCN at 298 K. The dotted lines are calculated by the Marcus equation [Eq. (1)] with $\lambda=0.50$–0.77 eV ([Zn(TPP)]), $\lambda=1.19$–1.61 eV ([Zn(DPP)]), $\lambda=0.40$–0.77 eV ([Al(TPP)(PhCO*O*)]), and $\lambda=0.76$–1.24 eV ([Al(DPP)(PhCO*O*)]). The open square (□) in (b) indicates the rate constant of electron transfer from ^{1}[Al(TPP)(PhCO*O*)]* to anthraquinone in PhCN at 298 K, determined by fluorescence-quenching experiments (Figures S13 and S14 in the Supporting Information).

of the photoinduced electron transfer, because the distance (R_{DA}) between the donor and acceptor molecules is known to be inversely proportional to the solvent reorganization energy (λ_s), in accordance with Equation (4), in which e is the electric charge, ε_0 is the electric constant, r_D and r_A are the ionic radii of the donor and acceptor molecules, respectively, and ε_{op} and ε_s are the optical and static dielectric constants of the solvent, respectively.[35]

$$\lambda_s = \frac{e^2}{4\pi\varepsilon_0}\left(\frac{1}{2r_D}+\frac{1}{2r_A}-\frac{1}{R_{DA}}\right)\left(\frac{1}{\varepsilon_{op}}-\frac{1}{\varepsilon_s}\right) \quad (4)$$

The driving-force dependence of the λ values of photoinduced electron transfer from the triplet excited states of metalloporphyrins to *p*-benzoquinone derivatives is shown in Figure 5. The λ values of all the porphyrins increase linearly with the increasing driving force of the photoinduced electron transfer, as expected from reference [36]. Such an increase in the λ value has been considered as the main reason why the Marcus inverted region cannot be observed in intermolecular photoinduced electron-transfer reactions except for the case in which there is an exceptionally small reorganization energy of electron transfer.[33,37,38] The minimum λ value of TPP (0.50 eV) at $-\Delta G_{et} \approx 0$ is similar to the minimum λ value of intermolecular photoinduced electron-transfer reactions of a cofacial zinc porphyrin dimer (0.50 eV),[36] and also to the reported λ value of photoinduced electron transfer in the π complex between a cofacial free-base porphyrin dimer and a sandwiched acridinium ion (0.54 eV).[39] Thus, a planar porphyrin has a small reorganization energy in photoinduced electron-transfer oxidation when the porphyrin is in close contact with an electron acceptor at $-\Delta G_{et} \approx 0$, when the interaction between the electron donor and acceptor molecules is maximized according to the Mulliken theory of charge-transfer complexes. In such a case, the solvent reorganization energy is minimized, as expected from Equation (4). As the driving force of photoinduced electron transfer increases, the interaction between the electron donor and acceptor molecules becomes weaker when the R_{DA} value increases to afford a larger solvent reorganization energy in accordance with Equation (4).

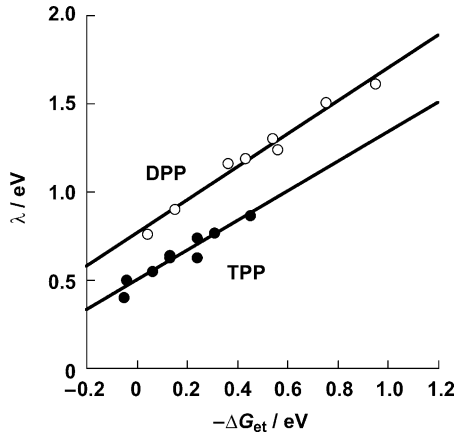

Figure 5. Dependence of λ on $-\Delta G_{et}$ for electron transfer from planar metalloporphyrins ([Zn(TPP)] and [Al(TPP)(PhCO*O*)]) (solid line with black circles), and saddle-distorted metalloporphyrins ([Zn(DPP)] and [Al(DPP)(PhCO*O*)]) (solid line with open circles) to various electron acceptors in PhCN at 298 K.

As shown in Figure 5, the λ values of planar metalloporphyrins without and with an axial ligand ([Zn(TPP)] and [Al(TPP)(PhCO*O*)], respectively) are similar to each other, but they are 0.27 eV smaller than those of the corresponding nonplanar metalloporphyrins ([Zn(DPP)] and [Al(DPP)(PhCO*O*)], respectively) when they are compared for the same driving force of photoinduced electron transfer. Thus, the λ values are not affected by the central metal or by the axial ligand as long as the electron transfer occurs at the porphyrin ring. In contrast, the conformational distortion of the porphyrin ring in DPP^{2-} results in a significant increase in the bond reorganization energy of the photoinduced electron-transfer oxidation of metalloporphyrins, as observed in the photoinduced electron-transfer reduction of diprotonated porphyrins.[27]

Aluminum porphyrins with anthraquinonecarboxylate axial ligand: The reactions of [Al(TPP)(OMe)] and [Al(DPP)(OH)] with anthraquinone-2-carboxylic acid (AqCOOH) in $CHCl_3$ afforded [Al(TPP)(AqCO*O*)] and [Al(DPP)(AqCO*O*)], respectively. Both [Al(TPP)(AqCO*O*)] and [Al(DPP)(AqCO*O*)] were well characterized by MALDI-TOF MS and ^{1}H NMR measurements (see Experimental Section). In the case of [Al(TPP)(AqCO*O*)], a single crystal was obtained as [Al(TPP)(AqCO*O*)(H_2O)] to allow us to determine the crystal structure, as shown in Figure 6, revealing the strong axial coordination of $AqCOO^-$ to the Al^{3+} ion of $Al(TPP)^+$ and the intracomplex π–π interactions between the porphyrin ligand and the $AqCOO^-$ ligand. The intracomplex π–π interactions were also observed between the centroid of the phenyl ring with the carboxyl group of the $AqCOO^-$ ligand and the *meso* carbon just below the centroid in the porphyrin ring (3.69 Å) in the face-to-face fashion, and the centroid of the quinone moiety of the $AqCOO^-$ ligand and the *ortho* carbon of the *meso*-phenyl group (3.70 Å) in the edge-to-face fashion. The bond length between the carboxylate oxygen of the $AqCOO^-$ ligand and the Al^{III} center is 1.889(3) Å, and that between the oxygen atom of the aqua

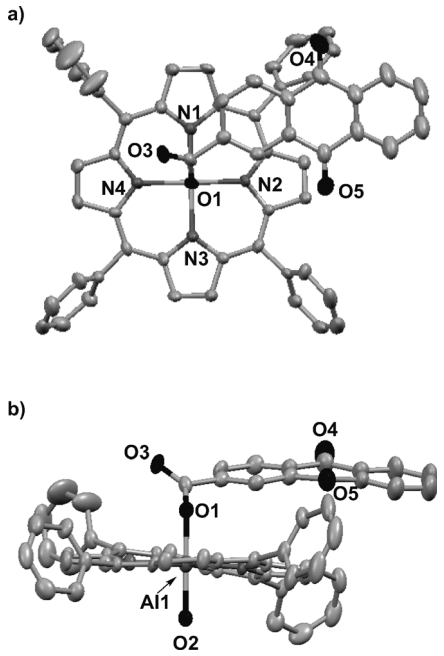

Figure 6. Crystal structure of [Al(TPP)(AqCO*O*)(H_2O)]·PhCN from different directions: a) top view; b) side view.

ligand and the Al^{III} center is 1.948(3) Å. The distance between the Al^{III} center and the carboxyl oxygen is comparable to those between Al^{III} centers and carboxylate oxygen atoms, which have been reported to be 1.861(3) Å for [Al(5,10,15,20-tetrakis(3,5-di-*tert*-butyl-phenyl)porphyrinato)(3-pyridine-carboxylato)], and 1.894(6) and 1.895(6) Å for [Al(5,10,15,20-tetrakis(3,5-di-*tert*-butyl-phenyl)porphyrinato)(4-pyridinecarboxylato)].[40]

In the case of the saddle-distorted [Al(DPP)(AqCO*O*)] complex, crystallized as [Al(DPP)(AqCO*O*)(H_2O)], the $AqCOO^-$ moiety is nearly perpendicular to the porphyrin ring (Figure 7). There is no intracomplex π–π interaction between the porphyrin ligand and the $AqCOO^-$ ligand. The $AqCOO^-$ moiety's motion is limited by the steric hindrance of the phenyl groups.

The coordination of the water molecule found in the crystal structures was assumed to be negligible in PhCN: no absorption spectral change was observed with the addition of water to the solutions of [Al(TPP)(AqCO*O*)] and [Al(DPP)(AqCO*O*)] in PhCN. The aqua ligand may be required for crystallization, as intermolecular hydrogen bonding was observed between the aqua ligand and the PhCN molecule of crystallization in both cases, and that between the aqua ligand and the carbonyl oxygen of the adjacent molecule in [Al(TPP)(AqCO*O*)(H_2O)] in the crystals (O(2)···O(3)′ = 2.593(4) Å and O(2)···N(PhCN) = 2.872(5) Å for [Al(TPP)-(AqCO*O*)(H_2O)]; O(aqua)···N(PhCN) = 2.785(6) Å for [Al(DPP)-(AqCO*O*)(H_2O)]). Thus, we refer to those complexes as five-coordinate compounds in the following sections in which the complexes are dealt with in PhCN solutions.

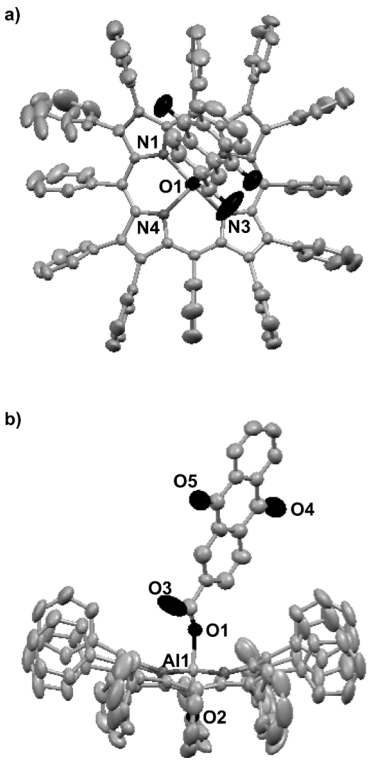

Figure 7. Crystal structure of [Al(DPP)(AqCO*O*)(H_2O)]·PhCN from different directions: a) top view; b) side view.

The redox potentials of [Al(TPP)(AqCO*O*)] were determined in PhCN by cyclic voltammetry (CV) and differential pulse voltammetry (DPV). The one-electron oxidation potential (E_{ox}) and the one-electron reduction potential (E_{red}) of [Al(TPP)(AqCO*O*)] were determined from the CV and DPV data in Figure 8 to be 0.75 V and −1.08 V (vs. SCE), respectively. Similarly, the E_{ox} and E_{red} values of [Al(DPP)-(AqCO*O*)] were determined to be 0.55 V and −1.09 V, respectively (Figure 9). On the basis of these redox potentials, the energy levels of the charge-separated (CS) states were determined as the difference between the first oxidation and first reduction potentials ([Al($TPP^{\bullet+}$)($AqCO*O*^{\bullet-}$)]: 1.83 eV; [Al($DPP^{\bullet+}$)($AqCO*O*^{\bullet-}$)]: 1.64 eV).

Photoinduced electron transfer in [Al(TPP)(AqCO*O*)] and [Al(DPP)(AqCO*O*)]: The energies of the singlet excited states of [Al(TPP)(AqCO*O*)] and [Al(DPP)(AqCO*O*)] were determined from the absorption and fluorescence spectra to be 1.96 and 1.88 eV, respectively (Figure 10 and Figures S15–S17 in the Supporting Information). Because the energies of the singlet excited states are higher than those

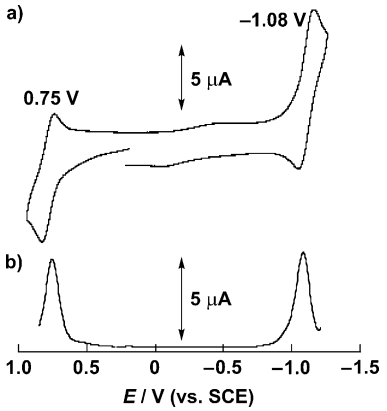

Figure 8. a) Cyclic voltammogram (scan rate: 0.5 $V s^{-1}$) and b) differential pulse voltammogram of [Al(TPP)(AqCO*O*)].

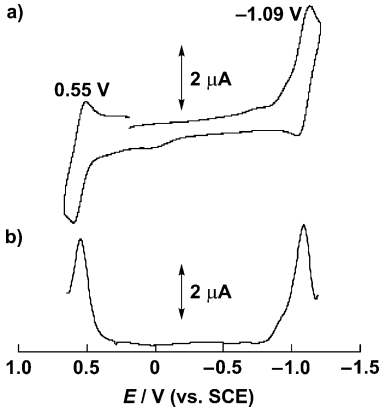

Figure 9. a) Cyclic voltammogram and b) differential pulse voltammogram of [Al(DPP)(AqCO*O*)].

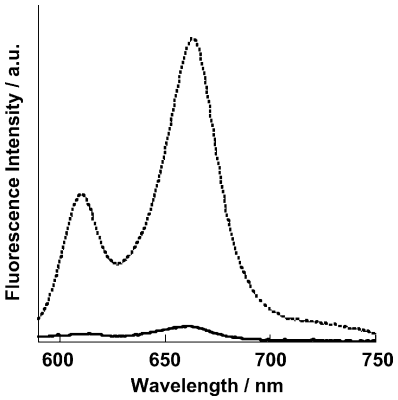

Figure 10. Fluorescence spectra of [Al(TPP)(AqCO*O*) (solid line) and [Al(TPP)(PhCO*O*)] (dotted line) in PhCN.

of the CS state energies, the fluorescence of [Al(TPP)-(AqCO*O*)] is significantly quenched as compared to that of [Al(TPP)(PhCO*O*)] because of electron transfer from the singlet excited state of $[Al(TPP)]^+$ ($^1[Al(TPP)^+]^*$) to $AqCOO^-$, as shown in Figure 10. Energy transfer from $^1[Al-(TPP)^+]^*$ to $AqCOO^-$ is unlikely to occur because the energy of the singlet excited state of anthraquinone[41] is significantly higher than that of $^1[Al(TPP)^+]^*$. Thus, electron transfer is the only quenching pathway of $^1[Al(TPP)^+]^*$. Similar results were obtained for [Al(DPP)(AqCO*O*)] (Figure S17 in the Supporting Information).

The photodynamics of intracomplex electron transfer from $^1[Al(DPP)^+]^*$ to $AqCOO^-$ were examined through femtosecond laser flash photolysis measurements. The femtosecond transient absorption spectrum of [Al(DPP)-(AqCO*O*)] in PhCN upon photoexcitation at 455 nm is shown in Figure 11a together with the time profile of the decay of the absorption at 546 nm (Figure 11b).

The transient absorption spectrum observed 3 ps after the laser excitation is assigned to the singlet excited state $^1[Al-(DPP)]^{+*}$ through comparison with that of [Al(DPP)-(PhCO*O*)] (Figure S18 in the Supporting Information), which has a broad absorption around 770 nm. At 200 ps, the broad absorption at around 700 nm due to $^1[Al(DPP)]^*$ disappears when the transient absorption spectrum agrees with that of the triplet excited state of [Al(DPP)(PhCO*O*)] (Figure S19 in the Supporting Information). In the case of [Al-(DPP)(PhCO*O*)], the conversion from $^1[Al(DPP)]^{+*}$ to $^3[Al(DPP)]^{+*}$ through intersystem crossing is slow, with a rate constant of $1.2\times10^9\ s^{-1}$ (Figure S18). The decay rate constant of $[^3Al(DPP)^*(AqCOO)]$ as determined from nanosecond laser flash photolysis (Figure S19, Supporting Information) is $1.1\times10^6\ s^{-1}$. This value is nearly the same as the decay rate constant of $[^3Al(DPP)^*(PhCOO)]$ to [Al-(DPP)(PhCO*O*)] ($1.1\times10^6\ s^{-1}$, Figure S20 in the Supporting Information). The much faster intersystem crossing in [Al-(DPP)(AqCO*O*)] as compared to [Al(DPP)(PhCO*O*)] indicates electron transfer from $^1[Al(DPP)]^{+*}$ to $AqCOO^-$. Although the charge-separated state could not be observed because of rapid back electron transfer to the triplet excited

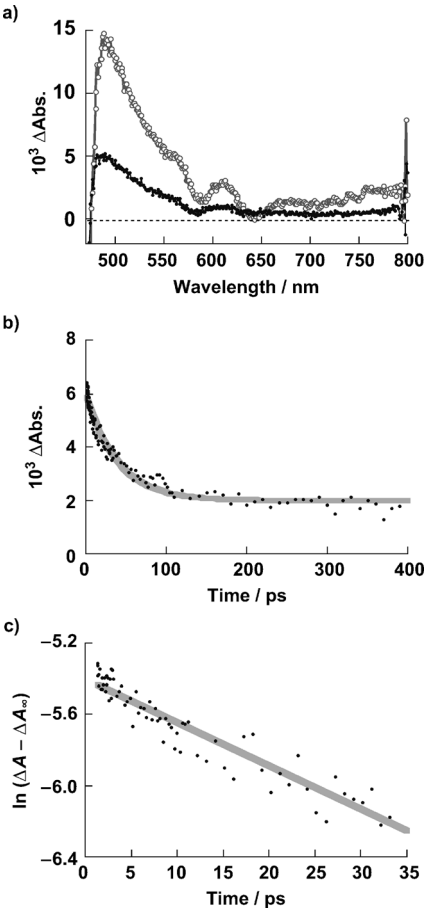

Figure 11. a) Transient absorption spectra of [Al(DPP)(AqCO*O*)] (3.0×10^{-5} M) in PhCN at 3.0 ps (gray line with open circles) and 200 ps (black line) after femtosecond laser excitation at 455 nm. b) Time profile at 546 nm. c) First-order plot.

state $[^3Al(DPP)^*(AqCOO)]$, electron transfer is the only pathway for the fast decay of $^1[Al(DPP)]^{+*}$, because energy transfer to $AqCOO^-$ is energetically impossible (vide supra).

Similar results were obtained for [Al(TPP)(AqCO*O*)], as shown in Figure 12. The rate constant of electron transfer from $^1[Al(TPP)]^{+*}$ to $AqCOO^-$ is determined from the decay time profile to be $1.3\times10^{10}\ s^{-1}$. In the case of [Al-(TPP)(PhCO*O*)], intersystem crossing from $^1[Al(TPP)]^{+*}$ to $^3[Al(TPP)]^{+*}$ is much slower, with a rate constant of $4.0\times10^8\ s^{-1}$ (Figure S21 in the Supporting Information). The decay rate constants of $[^3Al(TPP)^*(AqCOO)]$ and $[^3Al-(TPP)^*(PhCOO)]$ are determined to be $2.9\times10^3\ s^{-1}$ and $8.3\times10^3\ s^{-1}$, respectively, from the nanosecond laser flash photolysis measurements (Figures S22 and S23 in the Supporting Information).

The photodynamics and energetics of [Al(DPP)-(AqCO*O*)] and [Al(TPP)(AqCO*O*)] are summarized in Scheme 3. In both cases, efficient electron transfer occurs from the singlet excited state of Al porphyrins to the anthraquinone moiety, followed by rapid back electron transfer to produce the triplet excited state. The structure of [Al(DPP)-

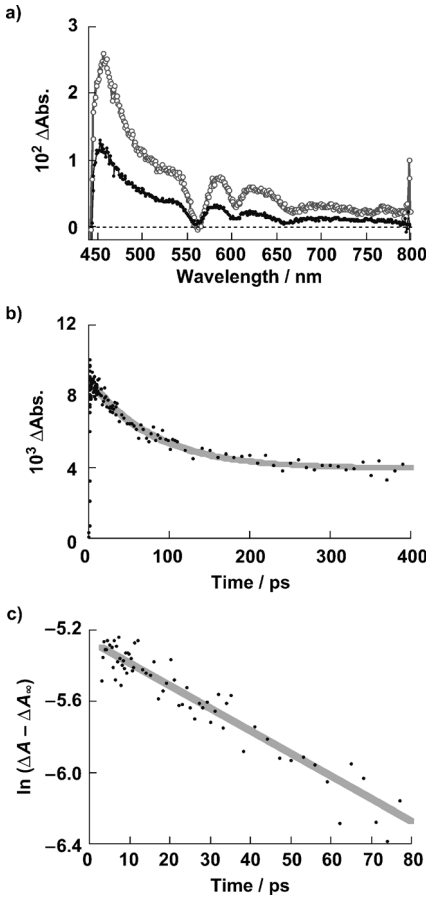

Figure 12. a) Transient absorption spectra of [Al(TPP)(AqCO*O*)] (3.0×10^{-5} M) in PhCN at 7.0 ps (gray line with open circles) and 400 ps (black line) after femtosecond laser excitation at 430 nm. b) Time profile at 527 nm. c) First-order plot.

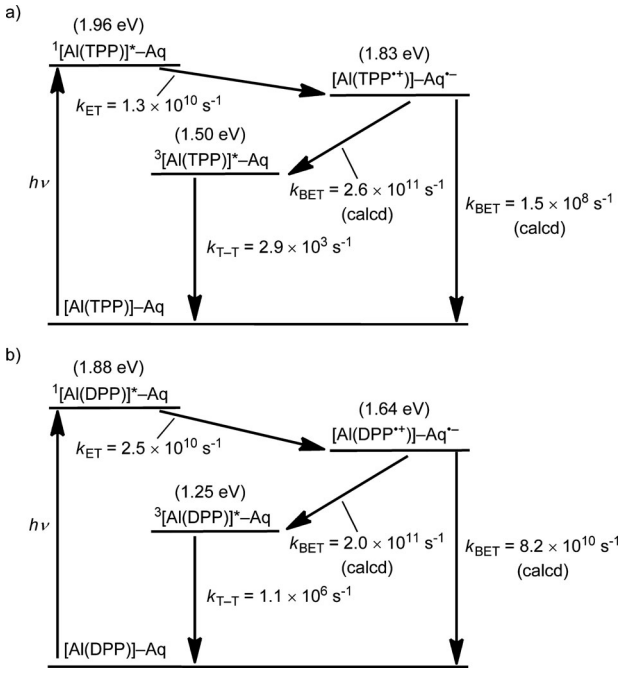

Scheme 3. Energy diagrams of [Al(TPP)(AqCO*O*)] and [Al(DPP)(AqCO*O*)].

(AqCO*O*)] is quite different from that of [Al(TPP)(AqCO*O*)], but the k_{ET} values of the two complexes are not very different. This indicates that intracomplex photoinduced electron-transfer reactions from Al porphyrins to $AqCOO^-$ moieties are adiabatic, because the rate constant of adiabatic electron transfer does not depend on the structures and electronic coupling of electron donors and acceptors.[10] Rate constants (k_{ET}) of adiabatic intramolecular electron-transfer reactions have been well predicted by the Marcus theory of electron transfer using Equation (5).[10,42,43]

$$k_{ET} = \frac{k_B T}{h}\exp\left(-\frac{(\Delta G^{o}_{ET}+\lambda)^2}{4\lambda k_B T}\right) \quad (5)$$

The resulting rate constants and driving forces of intracomplex photoinduced electron transfer were substituted into Equation (5) to determine the reorganization energies of the electron transfer. The λ values of [Al(TPP)(AqCO*O*)] and [Al(DPP)(AqCO*O*)] were determined to be 0.86 and 0.98 eV, respectively. As is the case with intermolecular electron transfer, the λ value of the saddle-distorted porphyrin is larger than that of the planar porphyrin. The rate constants of the back electron transfer from the CS states to triplet excited states of Al porphyrins or ground states were calculated from Equation (5). The calculated rate constants of back electron transfer from the CS states to triplet excited states of Al(TPP) and Al(DPP) in Scheme 3 are significantly larger than k_{ET}, in agreement with the experimental results shown in Figures 11 and 12. Thus, the observed photodynamics of [Al(TPP)(AqCO*O*)] and [Al(DPP)(AqCO*O*)] in Figures 11 and 12 can be well understood by assuming that intracomplex electron transfer is adiabatic, as in the case of intermolecular electron transfer.

Conclusion

The determination of reorganization energies of intermolecular photoinduced electron transfer from the triplet excited state of planar and nonplanar metalloporphyrins with and without axial ligand has allowed us to conclude that the bond reorganization energies are quite sensitive to the conformational distortion of the porphyrin ring, but are rather insensitive to the type of central metal or the axial ligand. On the other hand, the solvent reorganization energies increase with increasing driving force of the photoinduced electron-transfer reactions from the minimum value at $-\Delta G_{et}\approx0$. In the case of Al porphyrins, the axial ligand has been replaced by an electron acceptor ligand, that is, anthraquinonecarboxylate. The X-ray crystal structure of [Al(TPP)(AqCO*O*)] revealed strong axial coordination and the existence of intracomplex π–π interactions between the anthraquinone moiety and the porphyrin ring. In the case of the saddle-distorted [Al(DPP)(AqCO*O*)] complex, however, the $AqCOO^-$ moiety is nearly perpendicular to the porphyrin ring. The close proximity between the Al porphyrins and the $AqCOO^-$ moiety in both cases makes the intracomplex

photoinduced electron transfer and the back electron transfer adiabatic: the electron-transfer rate is determined solely by the driving force and reorganization energy of electron transfer, and not by geometric differences between the donor and acceptor moieties. Thus, the present study provides valuable insights for the rational design of efficient electron-transfer systems of metalloporphyrins.

Experimental Section

Materials: Chemicals were purchased from commercial sources and used without further purification, unless otherwise noted. 2,3,5,6-Tetramethyl-*p*-benzoquinone (Me_4Q), 2,5-dimethyl-*p*-benzoquinone (Me_2Q), 2-methyl-*p*-benzoquinone (MeQ), *p*-benzoquinone (Q), 2-chloro-*p*-benzoquinone (ClQ), 2,5-dichloro-*p*-benzoquinone (Cl_2Q), and *p*-chloranil (tetrachloro-*p*-benzoquinone; Cl_4Q), supplied by Aldrich, were purified by vacuum sublimation. Benzonitrile (PhCN) was purchased from Wako Pure Chemical Industries, Ltd. and purified by successive distillation over P_2O_5. CH_2Cl_2, used as a solvent, was distilled over CaH_2 before use. H_2TPP was purchased from a commercial source and used without further purification. H_2DPP was synthesized as reported previously.[44,45]

Synthesis of porphyrin complexes: [Al(TPP)(PhCO*O*)],[46] [Zn(TPP)],[47] and [Zn(DPP)][48] were synthesized on the basis of the procedure reported previously.

[Al(DPP)(PhCO*O*)]: Triethylaluminum (1.2 equiv, 0.15 mL, 1.9 M in toluene) was added to a solution of dodecaphenylporphyrin (H_2DPP) (350 mg, 0.29 mmol) in dry CH_2Cl_2 (300 mL) under an atmosphere of N_2. The solution was stirred at room temperature for 4 h. The reaction was quenched with 5 mL of methanol, and the stirring was continued overnight. The solvent was removed with a rotary evaporator. The residue was purified by column chromatography on activated alumina using CH_2Cl_2 as eluent. H_2DPP can be removed as the first fraction, and [Al(DPP)(OMe)] trapped at the top of the column was collected by using CH_2Cl_2/MeOH as the eluent. The solution was evaporated to dryness to obtain a purple solid (296 mg, 81% yield). Solid benzoic acid (5 equiv, 47.6 mg, 0.39 mmol) was added to a solution of [Al(DPP)(OMe)] (100 mg, 0.078 mmol) in $CHCl_3$ (50 mL). The resulting solution was stirred at room temperature for 24 h and then filtered to remove the excess benzoic acid. Hexane was added to the solution, yielding [Al(DPP)(PhCO*O*)] as a purple solid. Yield: 91% (97 mg). Elemental analysis calcd (%) for $C_{99}H_{65}O_2N_4Al{\cdot}C_6H_{14}$: C 86.63, H 5.47, N 3.85; found: C 86.50, H 5.32, N, 3.91; ^{1}H NMR ($CDCl_3$): $\delta=7.07$ (d, $J=7.3$ Hz, 1H; axial phenyl *p*-H), 7.01 (d, $J=7.2$ Hz, 8H; *meso*-phenyl *o*-H), 6.82 (t, $J=7.7$ Hz, 2H; axial phenyl *m*-H), 6.75–6.41 (m, 52H; *meso*-phenyl *m*-, *p*-H, β-phenyl H), 5.99 ppm (d, $J=7.1$ Hz, 2H; axial phenyl *o*-H); MALDI-TOF MS (matrix: dithranol): *m*/*z* calcd for $C_{99}H_{65}O_2N_4Al$ $[M]^+$: 1368.5; found: 1368.5; UV/Vis (in PhCN): λ_{max} (ε) = 455 (3.6×10^5), 585 (1.7×10^4), 634 nm (1.5×10^4 M^{-1} cm^{-1}).

[Al(TPP)(AqCO*O*)]: Solid anthraquinone-2-carboxylic acid (AqCOOH) (8 equiv, 400 mg, 1.60 mmol) was added to a solution of [Al(TPP)(OMe)] (137 mg, 0.21 mmol) in $CHCl_3$ (250 mL). The solution was stirred at room temperature for 12 h and then filtered to remove the excess AqCOOH. The solvent was removed with a rotary evaporator, yielding [Al(TPP)(AqCO*O*)] as a purple solid. Recrystallization of the solid from PhCN/hexane gave purple crystals, which were dried in vacuo at 100 °C for 12 h. Yield: 90% (171 mg). Elemental analysis calcd (%) for $C_{59}H_{35}O_4N_4Al{\cdot}H_2O{\cdot}0.5$ PhCN: C 78.16, H 4.14, N 6.56; found: C 78.07, H 4.22, N 6.47; ^{1}H NMR ($CDCl_3$): $\delta=9.09$ (s, 8H; β-phenyl H), 8.18 (d, $J=5.7$ Hz, 8H; *meso*-phenyl *o*-H), 8.05 (m, 2H; Aq5-, Aq8-H), 7.78–7.72 (m, 12H; *meso*-phenyl *m*-, *p*-H), 7.63 (m, 2H; Aq6-, Aq7-H), 7.34 (d, $J=8.1$ Hz, 1H; Aq4-H), 6.14 (s, 1H; Aq1-H), 5.43 ppm (d, $J=8.1$ Hz, 1H; Aq3-H); MALDI-TOF MS (matrix: dithranol): *m*/*z* calcd for $C_{59}H_{35}O_4N_4Al$ $[M]^+$requires 890.9; found: 890.1; UV/Vis (in PhCN): λ_{max} (ε) =: 320 (1.8×10^4), 426 (3.9×10^5), 561 (1.4×10^4), 601 nm (6.0×10^3 M^{-1} cm^{-1}).

[Al(DPP)(AqCO*O*)]: [Al(DPP)(OMe)] (150 mg, 0.12 mmol) was dissolved in CH_2Cl_2/acetone (3:1 v/v) with an aqueous solution of K_2CO_3 (5 mM, 1 mL), and the mixture was heated under reflux overnight. The solvent was evaporated, and the crude product was dissolved in CH_2Cl_2. After filtration, the filtrate was washed with water in a separating funnel and then dried over anhydrous sodium sulfate. Evaporation of the solvent gave a solid of [Al(DPP)(OH)]. [Al(DPP)(AqCO*O*)] was prepared using the same procedure as for [Al(TPP)(AqCO*O*)], but using [Al(DPP)(OH)] instead of [Al(TPP)(OMe)]. Recrystallization of the solid from CH_2Cl_2/hexane gave purple crystals, which were used for the elemental analysis. Then, the crystals were redissolved in PhCN, and the addition of hexane afforded plate-shaped crystals suitable for X-ray crystallographic analysis. Yield: 71% (126.2 mg). Elemental analysis calcd (%) for $C_{107}H_{67}O_4N_4Al{\cdot}C_6H_{14}$: C 85.58, H 5.15, N 3.53; found: C 85.21, H 5.00, N 3.57; ^{1}H NMR ($CDCl_3$): $\delta=8.23$–8.18 (m, 2H; Aq5-, Aq8-H), 7.78–7.73 (m, 3H; Aq1-, Aq6-, Aq7-H), 7.05 (d, $J=8.1$ Hz, 1H; Aq4-H), 7.03 (d, $J=6.9$ Hz, 8H; *meso*-phenyl *o*-H), 6.74–6.63 (m, 48H; *meso*-phenyl *p*-H, β-phenyl H), 6.45 (d, $J=8.1$ Hz, 1H; Aq3-H), 6.47–6.42 ppm (m, 8H; *meso*-phenyl *m*-H); MALDI-TOF MS (matrix: dithranol): *m*/*z* calcd for $C_{107}H_{67}O_4N_4Al$ $[M]^+$: 1499.7; found: 1500.1; UV/Vis (in PhCN): λ_{max} (ε) = 455 (3.6×10^5), 585 (1.7×10^4), 634 nm (1.5×10^4 M^{-1} cm^{-1}).

X-ray crystallographic measurements: A single crystal of [Al(TPP)(AqCO*O*)(H_2O)]·PhCN obtained from its PhCN/hexane solution was mounted in a loop with liquid paraffin. The measurements were performed on a Rigaku Mercury CCD area detector at −150 °C with graphite-monochromated $Mo_{K\alpha}$ radiation ($\lambda=0.71070$ Å) up to $2\theta_{max}=54.7°$. All calculations were performed using the Crystal Structure crystallographic software package,[49] and structure refinements were made by a direct method using SIR97.[50] The crystallographic data are summarized in Table 3. The Flack parameter was obtained as 0.1(2) by using 3442 Friedel pairs to confirm the absolute structure crystallographically.[51]

Table 3. X-ray crystallographic data for [Al(TPP)(AqCO*O*)(H_2O)]·PhCN and [Al(DPP)(AqCO*O*)(H_2O)]·PhCN.

	[Al(TPP)(AqCOO)-(H_2O)]·PhCN	[Al(DPP)(AqCOO)-(H_2O)]·PhCN
formula	$C_{66}H_{40}AlN_5O_5$	$C_{114}H_{74}AlN_5O_5$
fw	1010.05	1620.76
crystal system	tetragonal	triclinic
space group	$P4_1$	$P\bar{1}$
T [K]	123	298
a [Å]	13.1233(11)	13.4830(2)
b [Å]	13.1233(11)	16.3174(3)
c [Å]	28.758(3)	20.1155(4)
α [°]	90	90.1790(10)
β [°]	90	91.8430(10)
γ [°]	90	106.7710(10)
V [Å^3]	4952.7(7)	4234.77(13)
Z	4	2
R_1[a]	0.0478 [$I>2.0\sigma(I)$]	0.0656 [$I>2.0\sigma(I)$]
R_w[b]	0.0993 [$I>2.0\sigma(I)$]	0.1605 [$I>2.0\sigma(I)$]
GOF	0.824	1.049
Flack parameter	0.1(2)	–

[a] $R1=\Sigma||F_o|-|F_c||/\Sigma|F_o|$. [b] $R_w=[\Sigma(\omega(F_o^2-F_c^2)^2)/\Sigma\omega(F_o^2)^2]^{1/2}$. $\omega=1/[\sigma^2(F_o^2)+(0.0500P)^2+30.0000P$, in which $P=(\max(F_o^2,0)+2F_c^2)/3$.

The diffraction data of [Al(DPP)(AqCO*O*)(H_2O)]·PhCN were collected at ambient temperature from a small dark violet plate ($0.10\times0.07\times0.03$ mm^3), which was obtained from the crystallization solution (PhCN/hexane), immediately covered with a thin layer of Paratone-N oil and fixed to a glass rod with epoxy resign. Unlike the unprotected samples, which suffered from loss of solvent in less than 0.5 h, the protected crystal did not show any signs of degradation during data collection, and therefore no decay correction was applied. The X-ray diffraction data, up to $2\theta=52°$, were collected by ω-scans (0.5° frame width) with an APEX2 diffractometer (Bruker AXS),[52] using $Mo_{K\alpha}$ X-rays obtained from a ro-

tating anode source, a confocal multilayer X-ray mirror as the monochromator, and a CCD area detector. The integrated and scaled data were corrected empirically for absorption effects with SADABS ($\mu = 0.09\ mm^{-1}$).[53] The small size and the habit of the crystal, the low symmetry, and the large number of parameters required a longer exposure time (30 s), and nearly four-fold redundancy was achieved in one day. 54121 reflections were collected, of which 14836 unique reflections up to the cutoff limit of $2\theta = 50°$ with $R_{int} = 3.18\%$ were averaged for refinement. The structures were solved using direct methods,[54] and refined on F_{obs}^2 with SHELXL.[55] All non-hydrogen atoms were assigned anisotropic displacement parameters. To decrease the time cost of the refinement of the otherwise large number of variable parameters (1173 in the final cycle), the aromatic protons were set as riding bodies, whereas the water protons were refined freely. In the structure, the solvent benzonitrile (which is held only through a hydrogen bond to the coordinated water) and one part (one phenyl ring) of the polydentate ligand are heavily disordered, whereas the anthraquinone ligand shows smaller disorder. The treatment of the disorder necessitated the application of soft isotropic restraints (ISOR) to all atoms of the disordered phenyl ring (C1B1–C6B1, C1B2–C6B2) and the carboxylate group (O4, O3, and C35). Moreover, the ADPs of the atoms from the anchoring C−O bond were constrained to be similar. One other phenyl ring is strongly and nondiscretely disordered due to the puckering of the ring, indicating a dynamic process, and the disorder was refined to a 1:1 (0.52:0.48) ratio. One of the water protons is strongly hydrogen bonded to the nitrogen of the benzonitrile molecule (d(O5···N5) = 2.785(6) Å, $\measuredangle$(O5−H5···N5) = 173(4)°), and the other water proton forms an O5−H···π bond with a neighboring C1D–C6D phenyl ring (d(O5−Ct) = 3.87 Å). It should be noted that the carboxylate end of the anthraquinone-carboxylate ligand shows two distinct residual features close to C22, at appropriate distances corresponding to a disordered counterpart of C35−O4 from a component that is flipped around the Al1−O3 bond. However, although the residual peaks were clear, they were of insufficient intensity to be included in the refinement. The final cycle of refinement included 14836 reflections, and the 1173 parameters were refined by using 109 restraints to a goodness-of-fit of 1.049 and final residuals $R_1 = 0.0656$ and $wR_2 = 0.1605$ for $I > 2\sigma(I)$.

Spectroscopic measurements: Absorption spectra were measured on a Hewlett Packard 8453 diode array spectrophotometer at room temperature. Fluorescence spectra were obtained using an absolute PL quantum yield measurement system (Hamamatsu photonics, C9920–02). ^{1}H NMR spectra were measured on a JEOL AL-300 spectrometer and the chemical shifts (ppm) were determined by using the residual solvent peak as a reference. MALDI-TOF MS measurements were carried out on a Kratos Compact MALDI I (Shimadzu).

Phosphorescence measurements: The phosphorescence of N_2-saturated solutions of [Al(TPP)(PhCO*O*)], [Zn(DPP)], and [Al(TPP)(PhCO*O*)] in 2-methyltetrahydrofuran in quartz tubes (3 mm in diameter) in liquid nitrogen were measured using a SPEX Fluorolog τ3 fluorescence spectrophotometer by excitation at 559, 662, and 634 nm, respectively. A photomultiplier (Hamamatsu Photonics model R5509–72) was used to detect emission in the near-IR region.

Electrochemical measurements: Cyclic voltammetry (CV) and differential pulse voltammetry (DPV) were carried out on an ALS 630B electrochemical analyzer in deaerated PhCN containing 0.1 M [(nBu$_4$)N]PF$_6$ (TBAPF$_6$) as a supporting electrolyte at 298 K. A conventional three-electrode cell was used, with a platinum working electrode (surface area of 0.3 mm^2) and a platinum wire as the counter electrode. The Pt working electrode (BAS) was routinely polished with BAS polishing alumina suspension and rinsed with acetone before use. The potentials were measured with respect to the Ag/AgNO$_3$ (0.01 M) reference electrode. All potentials (vs. Ag/Ag$^+$) were converted to values versus SCE by adding 0.29 V.[56] All electrochemical measurements were performed under argon at atmospheric pressure.

Laser flash photolysis measurements: Measurements of nanosecond transient absorption spectra were made according to the following procedure. Degassed solutions of the metalloporphyrins and electron acceptors in PhCN were excited by a Panther OPO pumped Nd:YAG laser (Continuum, SLII-10, 4–6 ns fwhm) at 556 ([Zn(TPP)]), 559 ([Al(TPP)(PhCO*O*)]), 602 ([Zn(DPP)]), and 585 nm ([Al(DPP)(PhCO*O*)]). The resulting time-resolved transient absorption spectra were then measured using a continuous Xe lamp (150 W) and a photodiode (Hamamatsu 2949) as the probe light and detector, respectively. The output from the photodiode and photomultiplier tube was recorded using a digitizing oscilloscope (Tektronix, TDS3032, 300 MHz). The solutions were deoxygenated by Ar gas purging for 10 min prior to measurements. The rates of the photoinduced electron-transfer reactions were followed by the decay of the absorption maximum due to the triplet excited state of aluminum(III) or zinc(II) porphyrins under pseudo-first-order conditions. Pseudo-first-order rate constants were determined by a least-squares curve, fit using a microcomputer.

Femtosecond transient absorption spectroscopy experiments on solutions of [Al(TPP)(PhCO*O*)] and [Al(DPP)(PhCO*O*)] in deaerated PhCN were conducted using an ultrafast source (Integra-C,Quantronix Corp.), an optical parametric amplifier (TOPAS, Light Conversion Ltd.), and a commercially available optical detection system (Helios, provided by Ultrafast Systems LLC). The sources for the pump and probe pulses were derived from the fundamental output of Integra-C (780 nm, 2 mJ per pulse, and fwhm = 130 fs) at a repetition rate of 1 kHz. 75% of the fundamental output of the laser was introduced into TOPAS, which has optical frequency mixers resulting in a tunable range from 285 to 1660 nm; the rest of the output was used for white-light generation. Prior to generation of the probe continuum, a variable neutral density filter was inserted in the path in order to generate a stable continuum, then the laser pulse was fed to a delay line that provided an experimental time window of 3.2 ns with a maximum step resolution of 7 fs. In our experiments, a wavelength at 430 or 455 nm of TOPAS output, which is the fourth harmonic of the signal or idler pulses, was chosen as the pump beam. Because this TOPAS output consists not only of the desirable wavelength but also of unnecessary wavelengths, the latter were deviated using a wedge prism with a wedge angle of 18°. The desirable beam was irradiated at the sample cell with a spot size of 1 mm diameter, where it was merged with the white probe pulse in a close angle (<10°). The probe beam, after being passed through the 2 mm sample cell, was focused on a fiber optic cable that was connected to a CCD spectrograph to record the time-resolved spectra (410–800 nm). Typically, 2500 excitation pulses were averaged for 5 seconds to obtain the transient spectrum at a set delay time. Kinetic traces at appropriate wavelengths were assembled from the time-resolved spectral data.

Acknowledgements

We thank Prof. Kazuya Kikuchi and Taku Yamamoto for their help with the measurements of phosphorescence spectra. This work was supported by Grants-in-Aid (Nos. 20108010 and 21111501), a Global COE program, "the Global Education and Research Center for Bio-Environmental Chemistry" from the Japan Society of Promotion of Science (JSPS), Iketani Science and Technology Foundation, the Ministry of Education, Science, Technology of Japan, and by KOSEF/MEST through a WCU project (R31-2008-000-10010-0) from Korea.

[1] a) *Anoxygenic Photosynthetic Bacteria* (Eds.: R. E. Blankenship, M. T. Madigan, C. E. Bauer), Kluwer Academic Publishers, Dordrecht, **1995**; b) S. Hammes-Schiffer, *Acc. Chem. Res.* **2009**, *42*, 1881.
[2] a) G. T. Babcock, *Proc. Natl. Acad. Sci. USA* **1999**, *96*, 12971; b) H. B. Gray, J. R. Winkler, *Biochim. Biophys. Acta Bioenerg.* **2010**, *1797*, 1563.
[3] *Electron Transfer in Chemistry, Vols. 1–5* (Ed.: V. Balzani), Wiley-VCH, Weinheim, **2001**.
[4] *Photoinduced Electron Transfer* (Eds.: M. A. Fox, M. Chanon), Elsevier, Amsterdam, **1988**.
[5] L. Eberson, *Electron-Transfer Reactions in Organic Chemistry; Reactivity and Structure*, Springer, Heidelberg, **1987**.

[6] a) G. J. Kavarnos, N. J. Turro, *Chem. Rev.* **1986**, *86*, 401; b) A. Houmam, *Chem. Rev.* **2008**, *108*, 2180.
[7] a) R. Rathore, J. K. Kochi, *Adv. Phys. Org. Chem.* **2000**, *35*, 193; b) S. V. Rosokha, J. K. Kochi, *Acc. Chem. Res.* **2008**, *41*, 641.
[8] a) D. Gust, T. A. Moore, A. L. Moore, *Acc. Chem. Res.* **2009**, *42*, 1890; b) M. R. Wasielewski, *Acc. Chem. Res.* **2009**, *42*, 1910.
[9] a) S. Fukuzumi, *Org. Biomol. Chem.* **2003**, *1*, 609; b) S. Fukuzumi, *Bull. Chem. Soc. Jpn.* **2006**, *79*, 177; c) S. Fukuzumi, *Prog. Inorg. Chem.* **2009**, *56*, 49.
[10] a) R. A. Marcus, *Annu. Rev. Phys. Chem.* **1964**, *15*, 155; b) R. A. Marcus, *Angew. Chem.* **1993**, *105*, 1161; *Angew. Chem. Int. Ed. Engl.* **1993**, *32*, 1111; c) R. A. Marcus, N. Sutin, *Biochim. Biophys. Acta Rev. Bioenerg.* **1985**, *811*, 265.
[11] N. Sutin, *Prog. Inorg. Chem.* **1983**, *30*, 441.
[12] a) J. F. Endicott in *Comprehensive Coordination Chemistry II, Vol. 7* (Eds.: J. A. McCleverty, T. J. Meyer), Elsevier, Oxford, **2004**, pp. 657–730; b) D. M. Stanbury, *Adv. Inorg. Chem.* **2003**, *54*, 351.
[13] a) S. F. Nelsen, J. R. Pladziewicz, *Acc. Chem. Res.* **2002**, *35*, 247; b) S. Fukuzumi, C. L. Wong, J. K. Kochi, *J. Am. Chem. Soc.* **1980**, *102*, 2928; c) S. M. Hubig, J. K. Kochi, *J. Am. Chem. Soc.* **1999**, *121*, 1688; d) S. Fukuzumi, I. Nakanishi, T. Suenobu, K. M. Kadish, *J. Am. Chem. Soc.* **1999**, *121*, 3468; e) S. Fukuzumi, I. Nakanishi, K. Tanaka, T. Suenobu, A. Tabard, R. Guilard, E. Van Caemelbecke, K. M. Kadish, *J. Am. Chem. Soc.* **1999**, *121*, 785; f) Y.-M. Lee, H. Kotani, T. Suenobu, W. Nam, S. Fukuzumi, *J. Am. Chem. Soc.* **2008**, *130*, 434.
[14] a) L. Crovetto, S. E. Braslavsky, *J. Phys. Chem. A* **2006**, *110*, 7307; b) M. Murakami, K. Ohkubo, S. Fukuzumi, *Chem. Eur. J.* **2010**, *16*, 7820; c) P. Comba, S. Fukuzumi, H. Kotani, S. Wunderlich, *Angew. Chem.* **2010**, *122*, 2679; *Angew. Chem. Int. Ed.* **2010**, *49*, 2622; d) S. Fukuzumi, N. Fujioka, H. Kotani, K. Ohkubo, Y.-M. Lee, W. Nam, *J. Am. Chem. Soc.* **2009**, *131*, 17127.
[15] J. Deisenhofer, H. Michel, *Angew. Chem.* **1989**, *101*, 872; *Angew. Chem. Int. Ed. Engl.* **1989**, *28*, 829.
[16] a) G. von Jagow, W. D. Engel, *Angew. Chem.* **1980**, *92*, 684; *Angew. Chem. Int. Ed. Engl.* **1980**, *19*, 659; b) S. Fukuzumi, K. Okamoto, C. P. Gros, R. Guilard, *J. Am. Chem. Soc.* **2004**, *126*, 10441.
[17] *The Porphyrin Handbook, Vols. 1–20* (Eds.: K. M. Kadish, K. M. Smith, R. Guiard), Academic Press, New York, **2000/2003**.
[18] a) D. Gust, T. A. Moore, A. L. Moore, *Acc. Chem. Res.* **2001**, *34*, 40; b) M. R. Wasielewski, *Chem. Rev.* **1992**, *92*, 435; c) M. Jurow, A. E. Schuckmanb, J. D. Batteasb, C. M. Draina, *Coord. Chem. Rev.* **2010**, *254*, 2297.
[19] a) S. Fukuzumi, *Phys. Chem. Chem. Phys.* **2008**, *10*, 2283; b) S. Fukuzumi, T. Kojima, *J. Mater. Chem.* **2008**, *18*, 1427; c) S. Fukuzumi, T. Honda, K. Ohkubo, T. Kojima, *Dalton Trans.* **2009**, 3880.
[20] a) D. M. Guldi, G. M. A. Rahman, F. Zerbetto, M. Prato, *Acc. Chem. Res.* **2005**, *38*, 871; b) D. M. Guldi, *Pure Appl. Chem.* **2003**, *75*, 1069; c) D. M. Guldi, *Chem. Soc. Rev.* **2002**, *31*, 22.
[21] a) F. D'Souza, O. Ito, *Chem. Commun.* **2009**, 4913; b) F. D'Souza, O. Ito, *Coord. Chem. Rev.* **2005**, *249*, 1410; c) R. Chitta, F. D'Souza, *J. Mater. Chem.* **2008**, *18*, 1440.
[22] a) S. V. Bhosale, C. H. Jani, S. J. Langford, *Chem. Soc. Rev.* **2008**, *37*, 331; b) F. Scandola, C. Chiorboli, A. Prodi, E. Iengo, E. Alessio, *Coord. Chem. Rev.* **2006**, *250*, 1471; c) T. Kojima, T. Nakanishi, T. Honda, S. Fukuzumi, *J. Porphyrins Phthalocyanines* **2009**, *13*, 14.
[23] a) F. Wessendorf, B. Grimm, D. M. Guldi, A. Hirsch, *J. Am. Chem. Soc.* **2010**, *132*, 10786; b) M. E. El-Khouly, D. K. Ju, K.-Y. Kay, F. D'Souza, S. Fukuzumi, *Chem. Eur. J.* **2010**, *16*, 6193; c) J. L. Sessler, E. Karnas, S. K. Kim, Z. Ou, M. Zhang, K. M. Kadish, K. Ohkubo, S. Fukuzumi, *J. Am. Chem. Soc.* **2008**, *130*, 15256.
[24] a) A. Mateo-Alonso, C. Ehli, D. M. Guldi, M. Prato, *J. Am. Chem. Soc.* **2008**, *130*, 14938; b) A. Takai, M. Chkounda, A. Eggenspiller, C. P. Gros, M. Lachkar, J.-M. Barbe, S. Fukuzumi, *J. Am. Chem. Soc.* **2010**, *132*, 4477; c) F. D'Souza, N. K. Subbaiyan, Y. Xie, J. P. Hill, K. Ariga, K. Ohkubo, S. Fukuzumi, *J. Am. Chem. Soc.* **2009**, *131*, 16138.
[25] a) F. D'Souza, E. Maligaspe, K. Ohkubo, M. E. Zandler, N. K. Subbaiyan, S. Fukuzumi, *J. Am. Chem. Soc.* **2009**, *131*, 8787; b) T. Kojima, T. Honda, K. Ohkubo, M. Shiro, T. Kusukawa, T. Fukuda, N. Kobayashi, S. Fukuzumi, *Angew. Chem.* **2008**, *120*, 6814; *Angew. Chem. Int. Ed.* **2008**, *47*, 6712.
[26] K. Aoki, T. Goshima, Y. Kozuka, Y. Kawamori, N. Ono, Y. Hisaeda, H. D. Takagi, M. Inamo, *Dalton Trans.* **2009**, 119.
[27] T. Nakanishi, K. Ohkubo, T. Kojima, S. Fukuzumi, *J. Am. Chem. Soc.* **2009**, *131*, 577.
[28] M. O. Senge in *The Porphyrin Handbook, Vol. 1* (Eds.. K. M. Kadish, K. M. Smith, R. Guilard), Academic Press, New York, **2000**, p. 239.
[29] a) J. A. Shelnutt, X.-Z. Song, J.-G. Ma, S.-L. Jia, W. Jentzen, C. J. Medforth, *Chem. Soc. Rev.* **1998**, *27*, 31; b) J. A. Shelnutt in *The Porphyrin Handbook, Vol. 7* (Eds.: K. M. Kadish, K. M. Smith, R. Guilard), Academic Press, New York, **2000**, p. 167.
[30] P. K. Poddutoori, P. Poddutoori, B. G. Maiya, T. K. Prasad, Y. E. Kandrashkin, S. Vasil'ev, D. Bruce, A. van der Est, *Inorg. Chem.* **2008**, *47*, 7512.
[31] P. K. Poddutoori, A. S. D. Sandanayaka, T. Hasobe, O. Ito, A. van der Est, *J. Phys. Chem. B* **2010**, *114*, 14348.
[32] a) S. Fukuzumi, N. Nishizawa, T. Tanaka, *J. Org. Chem.* **1984**, *49*, 3571; b) H. Görner, *Photochem. Photobiol.* **2003**, *78*, 440.
[33] G. J. Kavarnos, *Fundamentals of photoinduced Electron Transfer*, Wiley-VCH, Weinheim, **1993**.
[34] A. Völcker, H.-J. Adick, R. Schmidt, H.-D. Brauer, *Chem. Phys. Lett.* **1989**, *159*, 103.
[35] a) B. S. Brunschwig, S. Ehrenson, N. Sutin, *J. Am. Chem. Soc.* **1984**, *106*, 6858; b) X. Shen, J. Lind, G. Merényi, *J. Phys. Chem.* **1987**, *91*, 4403; c) G. Merényi, J. Lind, X. Shen, *J. Phys. Chem.* **1988**, *92*, 134; d) X. Shen, J. Lind, T. E. Eriksen, G. Merényi, *J. Chem. Soc. Perkin Trans. 2* **1989**, 555.
[36] A. Takai, C. P. Gros, J. M. Barbe, R. Guilard, S. Fukuzumi, *Chem. Eur. J.* **2009**, *15*, 3110.
[37] a) D. Rehm, A. Weller, *Ber. Bunsen-Ges.* **1969**, *73*, 834; b) D. Rehm, A. Weller, *Isr. J. Chem.* **1970**, *10*, 259.
[38] a) S. Fukuzumi, S. Koumitsu, K. Hironaka, T. Tanaka, *J. Am. Chem. Soc.* **1987**, *109*, 305; b) S. Fukuzumi, K. Ohkubo, T. Suenobu, K. Kato, M. Fujitsuka, O. Ito, *J. Am. Chem. Soc.* **2001**, *123*, 8459; c) M. Murakami, K. Ohkubo, P. Mandal, T. Ganguly, S. Fukuzumi, *J. Phys. Chem. A* **2008**, *112*, 635.
[39] M. Tanaka, K. Ohkubo, C. P. Gros, R. Guilard, S. Fukuzumi, *J. Am. Chem. Soc.* **2006**, *128*, 14625.
[40] G. J. E. Davidson, L. A. Lane, P. R. Raithby, J. E. Warren, C. V. Robinson, J. K. M. Sanders, *Inorg. Chem.* **2008**, *47*, 8721.
[41] The energies of singlet and triplet excited states of anthraquinone (AQ) have been reported as 2.85 (^{1}AQ*) and 2.45 eV (^{3}AQ*). See: T. Itoh, M. Yamaji, H. Shizuka, *Spectrochim. Acta Part A* **2002**, *58*, 397.
[42] For examples of adiabatic intramolecular electron transfer, see: a) K. Lancaster, S. A. Odom, S. C. Jones, S. Thayumanavan, S. R. Marder, J.-L. Brédas, V. Coropceanu, S. Barlow, *J. Am. Chem. Soc.* **2009**, *131*, 1717; b) S. V. Rosokha, D.-L. Sun, J. K. Kochi, *J. Phys. Chem. A* **2002**, *106*, 2283; c) S. Fukuzumi, H. Kotani, K. Ohkubo, S. Ogo, N. V. Tkachenko, H. Lemmetyinen, *J. Am. Chem. Soc.* **2004**, *126*, 1600; d) L. Martín-Gomis, K. Ohkubo, F. Fernández-Lázaro, S. Fukuzumi, A. Sastre-Santos, *J. Phys. Chem. C* **2008**, *112*, 17694.
[43] For the boundary between adiabatic and nonadiabatic intermolecular electron transfer, see: a) S. F. Nelsen, D. A. Trieber II, M. A. Nagy, A. Konradsson, D. T. Halfen, K. A. Splan, J. R. Pladziewicz, *J. Am. Chem. Soc.* **2000**, *122*, 5940; b) S. F. Nelsen, M. N. Weaver, Y. Luo, J. R. Pladziewicz, L. K. Ausman, T. L. Jentzsch, J. J. O'Konek, *J. Phys. Chem. A* **2006**, *110*, 11665; c) J. P. Telo, S. F. Nelsen, Y. Zhao, *J. Phys. Chem. A* **2009**, *113*, 7730.
[44] C. J. Medforth, M. O. Senge, K. M. Smith, L. D. Sparks, J. A. Shelnutt, *J. Am. Chem. Soc.* **1992**, *114*, 9859.
[45] C.-J. Liu, W.-Y. Yu, S.-M. Peng, T. C. W. Mak, C.-M. Che, *J. Chem. Soc. Dalton Trans.* **1998**, 1805.
[46] G. J. E. Davidson, L. H. Tong, P. R. Raithby, J. K. M. Sanders, *Chem. Commun.* **2006**, 3087.

[47] M. E. El-Khouly, J. B. Ryu, K.-Y. Kay, O. Ito, S. Fukuzumi, *J. Phys. Chem. C* **2009**, *113*, 15444.
[48] a) N. Ono, H. Miyagawa, T. Ueta, T. Ogawa, H. Tani, *J. Chem. Soc. Perkin Trans. 1* **1998**, 1595; b) T. Kojima, R. Harada, *Acta Crystallogr. Sect. E* **2004**, *60*, 1097.
[49] CrystalStructure 3.7.0, Crystal Strucuture Analysis Package, Rigaku and Rigaku/MSC, The Woodlands, **2000–2005**.
[50] SIR 97 and SHELX 97, Programs for Crystal Structure Refinement, G. M. Sheldrick, University of Göttingen, Göttingen, **1997**.
[51] H. D. Flack, *Acta Crystallogr. Sect. A* **1983**, *39*, 876.
[52] Bruker AXS Inc., APEX2 (version 2.1-4) and SAINT (version 7.34A). Madison, **2007**.
[53] SADABS, G. M. Sheldrick, University of Göttingen, Göttingen, **1996**.
[54] G. M. Sheldrick, *Acta Crystallogr. Sect. A* **2008**, *64*, 112.
[55] SHELXL-97, G. M. Sheldrick, University of Göttingen, Göttingen, **1997**.
[56] C. K. Mann, K. K. Barnes, *Electrochemical Reactions in Non-aqueous Systems*, Mercel Dekker, New York, **1970**.

Received: February 14, 2011
Revised: July 17, 2011
Published online: September 23, 2011

